

# Disentangling Latent Embeddings with Sparse Linear Concept Subspaces (SLiCS)

Zhi Li<sup>1</sup>, Hau Phan<sup>1</sup>, Matthew Emigh<sup>2</sup>, and Austin J. Brockmeier<sup>1,3\*</sup>

<sup>1</sup>Department of Electrical & Computer Engineering, University of Delaware, USA

<sup>2</sup>Naval Surface Warfare Center, Panama City Division, Panama City, Florida, USA

<sup>3</sup>Department of Computer & Information Sciences, University of Delaware, USA

## Abstract

Vision-language co-embedding networks, such as CLIP, provide a latent embedding space with semantic information that is useful for downstream tasks. We hypothesize that the embedding space can be disentangled to separate the information on the content of complex scenes by decomposing the embedding into multiple concept-specific component vectors that lie in different subspaces. We propose a supervised dictionary learning approach to estimate a linear synthesis model consisting of sparse, non-negative combinations of groups of vectors in the dictionary (atoms), whose group-wise activity matches the multi-label information. Each concept-specific component is a non-negative combination of atoms associated to a label. The group-structured dictionary is optimized through a novel alternating optimization with guaranteed convergence. Exploiting the text co-embeddings, we detail how semantically meaningful descriptions can be found based on text embeddings of words best approximated by a concept’s group of atoms, and unsupervised dictionary learning can exploit zero-shot classification of training set images using the text embeddings of concept labels to provide instance-wise multi-labels. We show that the disentangled embeddings provided by our sparse linear concept subspaces (SLiCS) enable concept-filtered image retrieval (and conditional generation using image-to-prompt) that is more precise. We also apply SLiCS to highly-compressed autoencoder embeddings from TiTok and the latent embedding from self-supervised DINOv2. Quantitative and qualitative results highlight the improved precision of the concept-filtered image retrieval for all embeddings.

## 1 Introduction

Deep vision-language models trained on large datasets capture both visual and semantic features from the original inputs, encoding them into a dense vector space to generate image and text embeddings. These models are widely applied in tasks such as cross-modal retrieval and conditional generative modeling. In particular, the pre-trained CLIP model (Contrastive Language-Image Pre-Training) [Radford et al., 2021] uses separate image and text encoders to embed inputs into the same vector space using contrastive learning [Poole et al., 2019, Gutmann and Hyvärinen, 2010]. Even though CLIP embeddings are semantically rich, the dimensions of the dense vectors are not directly interpretable. For complex scene imagery, the ability to decompose an embedding vector into components corresponding to interpretable concepts would enable *concept-filtered* retrieval and conditional generation. Towards this goal, we propose Sparse Linear Concept Subspaces (SLiCS) to disentangle any given embedding vector into a set of component vectors, each a non-negative combination of basis vectors (atoms) defining a subspace for a coherent concept. The disentangled

\*This work relates to Department of Navy award N00014-24-1-2259 issued by the Office of Naval Research.

components provide an understanding of the distinct concepts present in an image. That is, each component subspace attempts to isolate and capture the possible variation of its associated concept within the embedding space. In order to associate a human-interpretable concept to each group, we exploit the fact that the image and text embedding spaces are aligned; we select descriptive words for each concept by using the word embeddings that are well-reconstructed by the concept’s atoms.

We assume that a deep image embedding encompasses the entire scene, densely preserving information about every object and background element. In retrieval, this holistic representation of the query image may not be ideal when we are interested in matching only a subset of aspects of the query image, as irrelevant aspects may adversely affect the retrieval. Suppose a query image contains multiple distinct concepts; then the embedding can be decomposed so that each concept-labeled component can be used to retrieve images similar to the aspects of the query image that are contained within that concept. For example, consider a complex query image containing a dog; to retrieve other images containing similar dogs, the “animal” component of the image embedding can be used to query the image database. Thus, concept-filtered retrieval, where the user can define which concepts should be focused on, has the potential to make image retrieval more flexible and precise. An overview of our proposed concept-filtered framework is presented in Fig. 1.

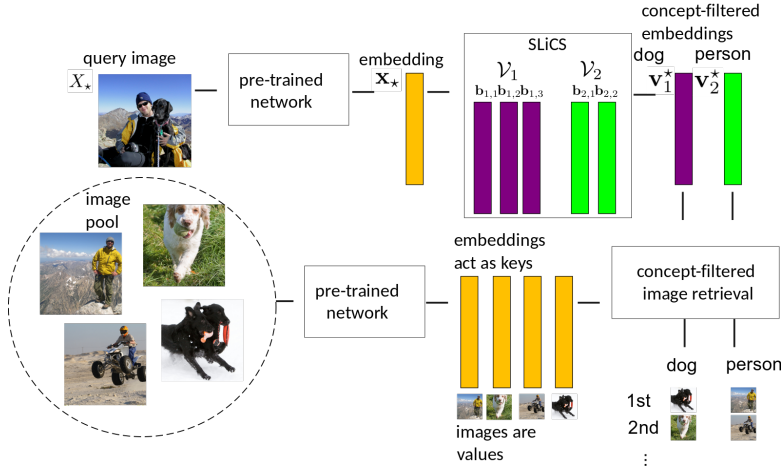


Figure 1: The pipeline of SLiCS-aided concept-filtered image retrieval. SLiCS decomposes a query image embedding  $x_*$  into multiple components  $v_1^*, v_2^*, \dots$ , one for each concept subspace  $\mathcal{V}_1, \mathcal{V}_2, \dots$ , such that  $x_* \approx v_1^* + v_2^* + \dots$ , where the  $j$ th component  $v_j^* \in \mathcal{V}_j$  is a non-negative combination of the  $M_j$  atoms  $b_{j,1}, \dots, b_{j,M_j}$  associated to the  $j$ th concept. Image retrieval can be performed on each disentangled component to retrieve the most similar concept-specific images.

Given a concept-labeled image dataset, SLiCS can learn a subspace for each concept. For vision-language models, the labels can be obtained from zero-shot classification of text embeddings of concepts. This provides for an unsupervised version of SLiCS.

However, SLiCS does not rely on the presence of text embeddings for supervised training. Deep vision embedding models trained using self-supervised objectives [Chen et al., 2020b,a, 2021, Caron et al., 2020, Oquab et al., 2023, Yu et al., 2024] and high-quality auto-encoders [Van Den Oord et al., 2017, Esser et al., 2021] with more compressed embeddings [Yu et al., 2024] also provide semantically rich embeddings, and can benefit from SLiCS-based disentangling for more precise retrieval. In summary, we propose SLiCS as an approach for learning to disentangle dense embeddings to enable concept-filtered retrieval and image generation in cases where the embedding can be directly decoded or used as a conditioning prompt.

## 2 Related Work

The emergence of CLIP has enabled various types of tasks involving the embedding of images and texts. Gandelsman et al. [2024] explore the interpretability of the intermediate representations in CLIP, breaking the vision transformer image encoder into patches and attention heads, trying to find

the text description for each attention head. However, it does not directly handle decomposition. Other methods implement decomposition with the help of text embeddings. Yuksekogonul et al. [2023] integrates the idea of subspaces into decomposition, although each concept is only spanned by one-word CLIP text embeddings. The projection of an image embedding onto a set of concepts gives a magnitude vector that can be further used in supervised classification. Similarly, SpLiCE [Bhalla et al., 2024], decomposes an image embedding on a set of fixed word embeddings with sparse coding. It operates in an unsupervised fashion, but the lack of subspaces construction limits the interpretation to instance level. Furthermore, both these methods are limited because of their reliance on the selection of word tokens. More similar to our approach, Kobs et al. [2023] use PCA to create a subspace with the guidance of a set of word embeddings that describe the same concept or aspect. Compared with these methods, SLiCS operates solely on image embeddings, only using text embeddings to construct pseudo-labels to aid the decomposition.

CLIP has inspired a number of image retrieval methods using text [Chaudhary et al., 2020] or multi-modal [Baldrati et al., 2022, Couairon et al., 2022, Liu et al., 2021] queries. Multi-modal approaches have used a combination of image and text to retrieve images similar to the contents of a query image modified by the provided query text. However, exploiting the CLIP image embeddings to perform concept-filtered retrieval remains unexplored.

More generally, our proposed SLiCS approach is a particular form of constrained dictionary learning, combining non-negativity of coefficients [Ding et al., 2008] with an assumption of group structure as in independent subspace analysis [Cardoso, 1998, Hyvärinen and Hoyer, 2000]. Non-negativity is important, as the inclusion of negative coefficients would make the interpretation more difficult. It would enable the negation of semantic meaning, as has been observed for word embeddings [Vylomova et al., 2015]. In the analysis of large language models, the sparse autoencoder [Huben et al., 2024] shows strong disentangling ability by retaining the top-K neuron activations at each iteration. However, unlike SLiCS, sparse autoencoders do not exploit group structure, and their post-hoc interpretation remains an open problem.

### 3 Method

Our proposed method, SLiCS, learns to disentangle vectors by decomposing them into a sparse sum of components lying in “subspaces” that are in fact positive cones, each defined by a non-negative combination of a group of vectors organized into a dictionary. When all the coefficients of a component group are zero, the component is zero, and the concept is inactive. The group structure enforced on the vectors makes the decomposition more structurally interpretable at the concept level, while at the same time maintaining the diversity within each disentangled subspace. In the supervised case with multi-label classes, the coefficients are forced to be inactive if a class is not present. Even with this known group activity, both the coefficients and the vector groups need to be learned. We propose a novel supervised dictionary learning algorithm with non-negative coefficients, inspired by the K-SVD algorithm [Aharon et al., 2006], which exploits rank-1 approximations to simultaneously update an atom and its contributions.

#### 3.1 Sparse Linear Concept Subspaces: Linear Synthesis Model

Let  $\phi : \mathcal{X} \rightarrow \mathbb{R}^d$  denote a pre-trained neural network that maps a query image  $X_\star \in \mathcal{X}$  to an embedding  $\mathbf{x}_\star = \phi(X_\star) \in \mathbb{R}^d$ . For  $S$  concepts, the embedding  $\mathbf{x}_\star$  is approximated as a sum of  $S$  components

$$\mathbf{x}_\star \approx \sum_{j=1}^S \mathbf{v}_j^\star = \sum_{j=1}^S \sum_{i=1}^{M_j} \alpha_{j,i} \mathbf{b}_{j,i} = \sum_{j=1}^S \mathbf{B}_j \boldsymbol{\alpha}_j = \mathbf{B} \boldsymbol{\alpha}, \quad (1)$$

where  $\mathbf{v}_j^\star \in \mathcal{V}_j \subseteq \mathbb{R}^d$  is the component residing in the corresponding positive cone  $\mathcal{V}_j$ ,  $\mathbf{B}_j = [\mathbf{b}_{j,1}, \dots, \mathbf{b}_{j,M_j}] \in \mathbb{R}^{d \times M_j}$  is the dictionary, each  $\mathbf{b}_{j,i}$ ,  $i \in \{1, \dots, M_j\}$  is an atom, and  $\boldsymbol{\alpha}_j \in \mathbb{R}_{\geq 0}^{M_j}$  is the non-negative coefficient vector, all associated to the  $j$ th concept. The combined dictionary is  $\mathbf{B} = [\mathbf{B}_j]_{j=1}^S \in \mathbb{R}^{d \times M}$ , with  $M = \sum_{j=1}^S M_j$ . The combined coefficient vector  $\boldsymbol{\alpha} = [\boldsymbol{\alpha}_j]_{j=1}^S \in \mathbb{R}_{\geq 0}^M$  has a group sparse pattern:  $\boldsymbol{\alpha}_j = \mathbf{0}$  implies that  $\mathbf{v}_j^\star = \mathbf{0}$  and the  $j$ th concept is inactive, whereas if the  $j$ th concept is active  $\|\mathbf{v}_j^\star\| > 0$  and  $\|\boldsymbol{\alpha}_j\| > 0$ . Hence, the support of  $\boldsymbol{\alpha}$  indicates the active subspaces in  $\mathbf{x}_\star$ .

Here  $\alpha_j$  is constrained to be non-negative, which is motivated by the fact that cosine similarity is used by CLIP to measure the similarity of embedding vectors. Embedding vectors pointing in opposite directions may represent semantic negation or dissimilar input images. Thus, an image embedding  $\mathbf{x}_*$  is considered to semantically include a concept only if its corresponding coefficient is positive. Furthermore, the enforcement of non-negativity reduces the “subspaces” to positive cones. For embeddings normalized to lie on a hypersphere, one can visualize the intersection of the positive cone and the hypersphere as a spherical polygon, as illustrated in a three-dimensional latent space case in Fig. 2(a) for  $S = 3$ . If  $\mathbf{x}_*$  lies in one of these spherical polygons, that means that it could

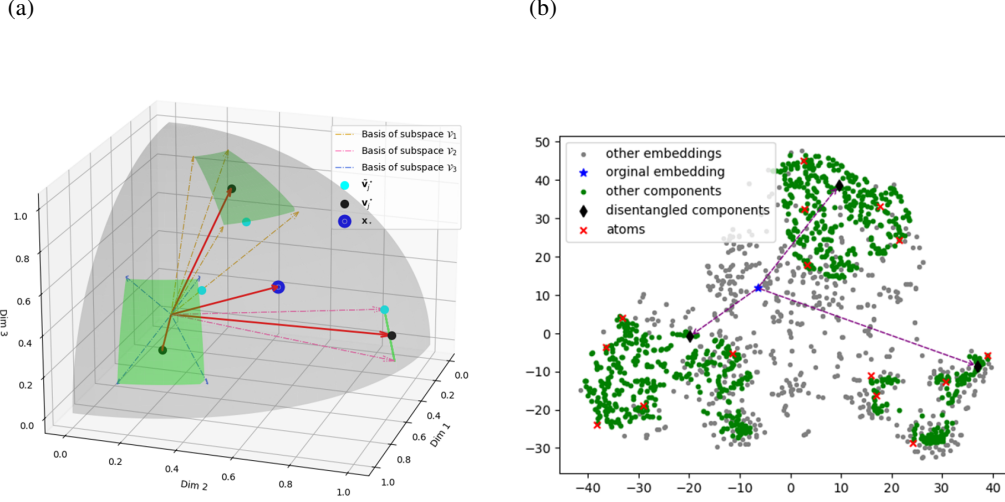


Figure 2: (a) On the left is an illustration of the “subspace” disentanglement of a three-dimensional latent space when  $S = 3$ . The gray surface denotes the unit sphere. The “subspaces” are the green surfaces, where the first and third concepts are defined by  $M_1 = M_3 = 4$  atoms and the second is defined by  $M_2 = 2$  atoms. The blue dot denotes  $\mathbf{x}_*$ . The three black dots denote  $\mathbf{v}_1^*, \mathbf{v}_2^*, \mathbf{v}_3^*$ . The three cyan dots denote  $\tilde{\mathbf{v}}_1^*, \tilde{\mathbf{v}}_2^*, \tilde{\mathbf{v}}_3^*$ , which are the nearest points to  $\mathbf{x}_*$  in the concept subspace. (b) On the right is a t-SNE visualization of disentangled subspaces by supervised SLiCS. An embedding of one point and its three components, lying in the three subspaces each defined by  $M_1 = M_2 = M_3 = 5$  atoms, are marked.

be described by a single active concept such that the atoms of the concept can fully describe it. An embedding vector of an image with multiple concepts could lie outside of these spherical polygons and be approximated by a non-negative combination of vectors from multiple spherical polygons. To illustrate this for a high-dimensional embedding space a t-SNE visualization [Van der Maaten and Hinton, 2008] of actual embeddings, their components, and atoms is shown in Fig. 2(b).

Out of convenience, we keep referring to the positive cones as “subspaces” in the following part of the work. (Note that the dictionaries are not constrained to be non-negative, so the problem is not a non-negative matrix factorization, but rather semi-non-negative matrix factorization.)

### 3.2 Sparse Linear Concept Subspaces: Disentanglement

Given the group-structured dictionary and the set of active concepts  $\mathcal{J}$ , the corresponding set of components can be obtained from  $\mathbf{x}_*$  by solving a non-negative least squares (NNLS) to obtain the coefficients.

$$\mathbf{v}_j^* = \mathbf{B}_j \alpha_j, \text{ where } [\alpha_j]_{j=1}^S = \arg \min_{[\mathbf{a}_j]_{j=1}^S \in \mathbb{R}_{\geq 0}^M} \|\mathbf{x}_* - \sum_{j \in \mathcal{J}} \mathbf{B}_j \mathbf{a}_j\|_2, \quad (2)$$

subject to  $\|\mathbf{a}_j\| = 0, \quad j \notin \mathcal{J}.$

NNLS is a convex quadratic program with linear constraints enforcing the non-negativity, which also yield sparsity among the coefficients [Slawski and Hein, 2013]. The minimization problem is not strictly convex, and may not have a unique solution if atoms in active concepts are linearly dependent. A strictly convex problem can be posed by regularizing the coefficients as in ridge regression [Hoerl and Kennard, 1970].



When a specific concept's component is desired, as in concept-filtered retrieval, one can perform a partial disentanglement by approximating  $\mathbf{x}_\star$  using only  $\mathbf{B}_j$ . This projects  $\mathbf{x}_\star$  to the  $j$ th concept's "subspace", yielding the vector in the subspace closest to the  $\mathbf{x}_\star$ ,

$$\tilde{\mathbf{v}}_j^\star = \mathbf{B}_j \boldsymbol{\alpha}_j = \arg \min_{\mathbf{v} \in \mathcal{V}_j} \|\mathbf{x}_\star - \mathbf{v}\|_2, \text{ where } \boldsymbol{\alpha}_j = \arg \min_{\mathbf{a} \geq 0} \|\mathbf{x}_\star - \mathbf{B}_j \mathbf{a}\|_2. \quad (3)$$

If different concept dictionaries are not orthogonal,  $\tilde{\mathbf{v}}_j^\star$  is generally different than  $\mathbf{v}_j^\star$ , as the latter considers all active concepts. This is illustrated in Fig. 2(a). In addition to being simpler, partial disentanglement performs better for concept-filtered retrieval, since  $\tilde{\mathbf{v}}_j^\star$  lies closer to  $x_\star$  and preserves more information in it (as shown later in Fig. 7).

When the active concepts are unknown, but only a few are assumed to be active, one can apply sparse coding algorithms with additional non-negativity constraints to estimate the unknown coefficients. In particular, Orthogonal Matching Pursuit [Mallat and Zhang, 1993, Rubinstein et al., 2008] or a group-structured variant [Swircszcz et al., 2009] are greedy approaches that iteratively add individual atoms or concepts, respectively, updating the coefficients after inclusion.

### 3.3 Supervised Dictionary Learning with Non-negative Coefficients

We now consider a supervised dictionary learning for SLiCS using a training set with labels  $\{(X_i, \mathbf{y}_i)\}_{i=1}^N$ , where  $\mathbf{y}_i \in \{0, 1\}^S$  is a  $S$ -dimensional binary label vector that indicates the presence of each concept in image  $X_i \in \mathcal{X}$ .  $\mathbf{X} = [\mathbf{x}_i]_{i=1}^N \in \mathbb{R}^{d \times N}$  is the concatenation of the training set mapped to the embedding space,  $\mathbf{x}_i = \phi(X_i)$ . Let  $\mathcal{I}_j = \{i : y_{ij} = 1\}$  denote the index set that contains the indices for which concept  $j$  is present. Supervised SLiCS minimizes the mean squared reconstruction error of the approximation (1), which can be compactly written as

$$\begin{aligned} \min_{\mathbf{B}, \mathbf{A}} \quad & \frac{1}{N} \|\mathbf{X} - \mathbf{B}\mathbf{A}\|_F^2 \\ \text{s.t.} \quad & \boldsymbol{\alpha}_j^i = \mathbf{0} \quad \text{if } y_{ij} = 0, \end{aligned} \quad (4)$$

where  $\mathbf{A} = [\boldsymbol{\alpha}_j^i]_{i=1}^N \in \mathbb{R}_{\geq 0}^{M \times N}$  denotes the coefficient matrix.

To solve this problem, we develop a supervised dictionary learning algorithm under a non-negative coefficient constraint, based on the K-SVD algorithm [Aharon et al., 2006]. K-SVD is an unsupervised dictionary learning algorithm that iteratively solves  $\mathbf{A}$  using greedy sparse coding algorithms, such as orthogonal matching pursuit [Pati et al., 1993], and solves  $\mathbf{B}$  by separately updating each atom using a rank-1 truncated SVD of the residual error matrix formed from the subset of the training set where the atom is active by removing the atom's contribution to the approximation, while fixing the contribution of other atoms. This update also simultaneously updates the corresponding coefficients of the updated atom.

In our case, we enforce group sparsity according to the labels and enforce non-negativity constraints on  $\boldsymbol{\alpha}^i$ . The solution is given by non-negative least squares (NNLS) on the supported concepts

$$\begin{aligned} \boldsymbol{\alpha}^i = \arg \min_{\{\mathbf{a}_j\}_{j=1}^S \in \mathbb{R}_{\geq 0}^M} \quad & \|\mathbf{x}_i - \sum_{j=1}^S \mathbf{B}_j \mathbf{a}_j\|_2, \\ \text{subject to} \quad & (1 - y_{ij}) \|\mathbf{a}_j\| = 0, \quad j \in \{1, \dots, S\}, \end{aligned} \quad (5)$$

where the constraint ensures that the coefficients are zero for inactive concepts  $y_{ij} = 0$ . Given the coefficients  $\mathbf{A} = [\boldsymbol{\alpha}_j^i]_{i=1}^N$ , the atom is updated to improve the approximation. For the  $m$ th atom, the optimization problem is

$$\min_{\mathbf{b}} \sum_{l \in \mathcal{L}_m} \min_{\beta_l \geq 0} \underbrace{\|\mathbf{x}_l - \sum_{k \neq m} \mathbf{b}_k A_{kl} - \beta_l \mathbf{b}\|_2}_{\mathbf{e}_l}^2 = \min_{\mathbf{b}, \beta \geq 0} \|\mathbf{E} - \mathbf{b}\beta\|_F^2, \quad (6)$$

where  $\mathbf{E} = [\mathbf{e}_l]_{l \in \mathcal{L}_m}$  denotes the residual error matrix and  $\mathcal{L}_m = \{l \in \{1, \dots, N\} : A_{ml} \neq 0\}$  is the subset of the training set where the atom is active. Without the non-negativity constraints, the rank-1 truncated SVD of the residual error provides the optimal update of the atom and coefficients, by the Eckart–Young–Mirsky theorem,

$$\tilde{\mathbf{b}}_m \tilde{\beta} = \sigma_1 \mathbf{u}_1^L \mathbf{u}_1^{R\top} = \arg \min_{\hat{\mathbf{E}}: \text{rank}(\hat{\mathbf{E}})=1} \|\mathbf{E} - \hat{\mathbf{E}}\|_F, \quad (7)$$

where  $\mathbf{E} = \mathbf{U}^L \Sigma \mathbf{U}^{R\top}$  is the SVD,  $\tilde{\mathbf{b}}_m = \mathbf{u}_1^L$  is left singular vector paired with the largest singular value  $\sigma_1$ , and  $\tilde{\beta} = \sigma_1 \mathbf{u}_1^{R\top}$  corresponding right singular vector scaled by the singular value.

However, as this does not ensure non-negativity of coefficients it may no longer be the optimal solution to minimize the reconstruction error. In fact, finding an optimal solution with non-negativity, which is the rank-1 semi-non-negative matrix factorization problem, is NP-Hard [Gillis and Kumar, 2015]. Nonetheless, we start from the rank-1 SVD, selecting the polarity of the atom through a simple majority rule that we prove is guaranteed to be the optimal polarity (details are given in Section 3.3.1), and apply thresholding to ensure coefficients are non-negative. While this SVD-based update is still heuristic, the simultaneous update of atom and coefficient converges, as we show in Section 3.3.2. Empirically, the simultaneous update is more efficient than an alternating update we discuss in Appendix A.

While the initialization was not specified in the original K-SVD paper, here we apply truncated SVD to embeddings of the  $j$ th concept  $[\mathbf{x}_i]_{i \in \mathcal{I}_j} = \mathbf{U}^L \Sigma \mathbf{U}^{R\top}$ , taking the columns of  $\mathbf{U}^L$  corresponding to the top  $M_j$  singular values, choosing the optimal polarity for each, to initialize the  $j$ th block  $\mathbf{B}_j$ .<sup>2</sup> One could select  $M_j$  to ensure a maximum error fraction as is done in PCA. For simplicity, we assume all dictionaries have the same size  $d_0 = M_j$ ,  $j \in \{1, \dots, S\}$  ( $M = S \cdot d_0$  total atoms) and vary  $d_0$ . Finally, we run for a fixed number  $T$  of updates, but a stopping criterion based on error reduction (possibly on a validation set) or the norm of the difference of atom updates can be used. The complete set of steps is described in Alg. 1.

If the training set is too large to fit in memory, each iteration could be treated as an epoch and broken into disjoint mini-batches. If  $\mathcal{B} \subset \{1, \dots, N\}$  is a batch of indices, then coefficients are estimated on this batch  $[\alpha^i]_{i \in \mathcal{B}}$  and then all atoms (and corresponding coefficients) that are active on the batch are updated. The training set is shuffled among the batches after each epoch.

---

**Algorithm 1** Supervised SLiCS dictionary learning

---

**Require:** Embedding matrix  $\mathbf{X} \in \mathbb{R}^{d \times N}$ , cardinality of each dictionary  $M_1, \dots, M_S$  with  $M = \sum_{j=1}^S M_j$ , concept indices from labels,  $\mathcal{I}_j \subset \{1, \dots, N\}$ ,  $j \in \{1, \dots, S\}$ , max iterations  $T$

**Ensure:** Dictionary  $\mathbf{B} = [\mathbf{B}_j]_{j=1}^S = [\mathbf{b}_m]_{m=1}^M$

**for**  $j = 1$  to  $S$  **do**

    Initialize  $\mathbf{B}_j \leftarrow [p_k^* \mathbf{u}_k^L]_{k=1}^{M_j}$  from the rank- $M_j$  truncated SVD of  $[\mathbf{x}_i]_{i \in \mathcal{I}_j} \approx \sum_{k=1}^{M_j} \sigma_k \mathbf{u}_k^L \mathbf{u}_k^{R\top}$

    with optimal signs  $p_k^* = \begin{cases} 1 & \|\max(0, \mathbf{u}_k^R)\|_2 \geq \|\max(0, -\mathbf{u}_k^R)\|_2 \\ -1 & \text{otherwise} \end{cases}$

**end for**

**for**  $t = 1$  to  $T$  **do**

**for**  $i = 1$  to  $N$  **do**

        Solve  $\alpha^i = [\alpha_j^i]_{j=1}^S$  using NNLS on supported concepts,  $\alpha_j^i = 0$  if  $i \notin \mathcal{I}_j$ , as in (5)

**end for**

$\mathbf{A} \leftarrow [\alpha^i]_{i=1}^N$

**for**  $m = 1$  to  $M$  **do**

        Find the support indices  $\mathcal{L}_m \leftarrow \{l \in \{1, \dots, M\} : A_{ml} \neq 0\}$  of the  $m$ th row of  $\mathbf{A}$

        Calculate the residual error without the  $m$ th atom  $\mathbf{E} \leftarrow [\mathbf{x}_l - \sum_{k \neq m} \mathbf{b}_k A_{kl}]_{l \in \mathcal{L}_m}$

        Obtain rank-1 truncated SVD of residual error  $\mathbf{E} \approx \tilde{\mathbf{b}}_m \tilde{\beta}$ ,

        Compute the optimal sign  $p^* = \begin{cases} 1 & \|\max(0, \tilde{\beta})\|_2 \geq \|\max(0, -\tilde{\beta})\|_2 \\ -1 & \text{otherwise} \end{cases}$

        Update the atom  $\mathbf{b}_m \leftarrow p^* \tilde{\mathbf{b}}_m$

        Update the active coefficients  $\mathbf{A}_{m\mathcal{L}_m} \leftarrow \max(0, p^* \tilde{\beta}) = \arg \min_{\beta \geq 0} \|\mathbf{E} - \mathbf{b}_m \beta\|_F$

**end for**

**end for**

---

<sup>2</sup>One could also initialize each block in the dictionary in the same way as K-means is initialized, using random samples from  $\mathcal{I}_j$  as the atoms in the  $j$ th block. We test two different methods, and in practice, the SVD-based approach performs consistently better in terms of the approximation error of the final dictionary.

### 3.3.1 Optimal sign for atom update

The optimality of the majority rule follows from the fact that the non-negative least squares problem can be decomposed into solving one entry of  $\mathbf{A}_{m\mathcal{L}_m} = [A_{ml}]_{l \in \mathcal{L}_m}$  at a time. Since the solution of non-negative linear regression is given by the active set method [Bro and De Jong, 1997], the entry is either included in the active set if it is non-negative, or not included if it is negative. Hence, the optimal non-negative  $\beta^*$  is obtained by setting the negative coefficient to zero. Additionally, the rank-1 SVD already guarantees the optimal result of ordinary linear regression  $\tilde{\beta}$ , which allows us to prove that the majority sign rule reduces the error. We begin by decomposing the norm of the error of the rank-1 approximation of the residual,

$$\begin{aligned} \|\mathbf{E} - \tilde{\mathbf{b}}_m \tilde{\beta}\|_F^2 &= \sum_{l \in \mathcal{L}_m} \|\mathbf{e}_l - \tilde{\mathbf{b}}_m \tilde{\beta}_l\|_2^2 = \sum_{l \in \mathcal{L}_m} \left( \|\mathbf{e}_l\|_2^2 + \underbrace{\|\tilde{\mathbf{b}}_m \tilde{\beta}_l\|_2^2}_{\tilde{\beta}_l^2} - 2 \underbrace{\tilde{\beta}_l \mathbf{e}_l^\top \tilde{\mathbf{b}}_m}_{\tilde{\beta}_l^2} \right) \\ &= \sum_{l \in \mathcal{L}_m} \left( \|\mathbf{e}_l\|_2^2 - \tilde{\beta}_l^2 \right) = \sum_{l \in \mathcal{L}_m} \left( \|\mathbf{e}_l\|_2^2 - \max(0, \tilde{\beta}_l)^2 - \max(0, -\tilde{\beta}_l)^2 \right) \\ &= \|\mathbf{E}\|_F^2 - \|\max(0, \tilde{\beta})\|_2^2 - \|\max(0, -\tilde{\beta})\|_2^2, \end{aligned} \quad (8)$$

where the simplifications follow from the fact that the optimal least-square coefficient  $\tilde{\beta}_l = \mathbf{e}_l^\top \tilde{\mathbf{b}}_m$  is simply the inner-product with the unit vector  $\tilde{\mathbf{b}}_m$ . This can also be seen from the SVD, since

$$\begin{aligned} \left[ \tilde{\mathbf{b}}_m^\top \mathbf{e}_l \right]_{l \in \mathcal{L}_m} &= \tilde{\mathbf{b}}_m^\top \mathbf{E} = \tilde{\mathbf{b}}_m^\top \mathbf{U}^L \Sigma \mathbf{U}^{R\top} = \sigma_1 \mathbf{u}_1^{R\top} = \tilde{\beta} \\ \tilde{\mathbf{b}}_m^\top \mathbf{e}_l &= \tilde{\beta}_l. \end{aligned} \quad (9)$$

For arbitrary sign  $p \in \{-1, 1\}$ , and given the non-negative thresholding operator  $(\cdot)_+ = \max(0, \cdot)$ , we note that

$$\sum_{l \in \mathcal{L}_m} \min_{\beta \geq 0} \|\mathbf{e}_l - p \tilde{\mathbf{b}}_m \beta\|_2^2 = \sum_{l \in \mathcal{L}_m} \|\mathbf{e}_l - p \tilde{\mathbf{b}}_m (p \mathbf{e}_l^\top \tilde{\mathbf{b}}_m)_+\|_2^2 = \|\mathbf{E} - p \tilde{\mathbf{b}}_m (p \tilde{\beta})_+\|_2^2, \quad (10)$$

since the optimal non-negative least-square coefficient is the non-negative projection of the optimal least squares component  $\beta_l = \max(0, p \mathbf{e}_l^\top \tilde{\mathbf{b}}_m)$ . To show the optimality of  $p^*$  defined by the majority sign, the non-negative approximation can be expanded as in (8), yielding

$$\begin{aligned} \|\mathbf{E} - p \tilde{\mathbf{b}}_m (p \tilde{\beta})_+\|_F^2 &= \sum_{l \in \mathcal{L}_m} \|\mathbf{e}_l - p \tilde{\mathbf{b}}_m (p \tilde{\beta}_l)_+\|_2^2 \\ &= \sum_{l \in \mathcal{L}_m} \left( \|\mathbf{e}_l\|_2^2 + \underbrace{p^2}_{1} \underbrace{\|\tilde{\mathbf{b}}_m (p \tilde{\beta}_l)_+\|_2^2}_{(p \tilde{\beta}_l)_+^2 \|\tilde{\mathbf{b}}_m\|_2^2 = (p \tilde{\beta}_l)_+^2} - 2 \underbrace{p (p \tilde{\beta}_l)_+ \tilde{\mathbf{b}}_m^\top \mathbf{e}_l}_{p (p \tilde{\beta}_l)_+ \tilde{\beta}_l = (p \tilde{\beta}_l)_+^2} \right) \\ &= \sum_{l \in \mathcal{L}_m} \left( \|\mathbf{e}_l\|_2^2 - (p \tilde{\beta}_l)_+^2 \right) \\ &= \|\mathbf{E}\|_F^2 - \|(p \tilde{\beta})_+\|_2^2 \\ &\geq \|\mathbf{E}\|_F^2 - \max(\|\tilde{\beta}\|_2^2, \|(-\tilde{\beta})\|_2^2) = \|\mathbf{E} - p^* \tilde{\mathbf{b}}_m (p^* \tilde{\beta})_+\|_F^2, \end{aligned} \quad (11)$$

where the following equality was used, which holds for any scalar  $\beta$

$$\begin{aligned} p(p\beta)_+ &= p\beta(p\beta)_+ = \begin{cases} (p\beta)^2, & (p\beta)_+ \geq 0 \\ 0, & (p\beta)_+ < 0 \end{cases} \\ &= (p\beta)_+^2. \end{aligned} \quad (12)$$

This shows that  $p^*$  computed by the majority rule is always the optimal sign.

### 3.3.2 Convergence

The first step in each iteration, the coefficient update, always reduces the reconstruction error as non-negative linear regression is a convex minimization problem with a unique global minimum. The update of each atom (and coefficients) can be made contingent on improving the approximation, i.e., the atom update can be skipped if the newly found coefficients and the new atom with optimal sign do not provide a better rank-1 approximation compared to the original atom and previous coefficients. Mathematically, the update improves the approximation if

$$\|\mathbf{E} - p^* \tilde{\mathbf{b}}_m(p^* \tilde{\boldsymbol{\beta}})_+\|_F^2 = \sum_{l \in \mathcal{L}_m} \|\mathbf{x}_l - \sum_{k \neq m} \mathbf{b}_k A_{kl} - p^* \tilde{\mathbf{b}}_m(p^* \tilde{\boldsymbol{\beta}}_l)_+\|_2^2 \leq \sum_{l \in \mathcal{L}_m} \|\mathbf{x}_l - \sum_k \mathbf{b}_k A_{kl}\|_2^2. \quad (13)$$

With this check, the algorithm is a cyclic minimizer [Stoica and Selen, 2004], and thus is guaranteed to converge since both stages reduce the error.

In practice, we let the algorithm proceed with an atom update without checking if it will increase the reconstruction error, as it may end up achieving a better local minimum.

Finally, we note that an alternative is to use block-coordinate descent on the atom and coefficient update, which will always reduce the error (see Section A); however, in simulations our simultaneous approach using SVD and thresholding with optimal sign leads to a better approximation.

### 3.4 Unsupervised Dictionary Learning of Concepts via Zero-shot Concept Classification

While the labels provide direct guidance on the group sparsity in the supervised cases, we also implement an essentially unsupervised version by exploiting the image-text alignment of CLIP if the set of concepts and the expected number of active concepts are known. Suppose we have the CLIP text embeddings  $\{\mathbf{w}_i\}_i^S$  of the  $S$  concept words across the templates (for example, “This is a picture of {word}”). The cosine similarity between an image embedding and each text embedding serves as a measurement of how close the word is to the image. In zero-shot classification, the concept with the highest score is the prediction. Here, since there are multiple concepts presented in each image we pick the highest  $\tilde{S}$  concepts as active. Thus, a pseudo-label is formed to enable the unsupervised SLiCS with the same algorithm as the supervised one.

### 3.5 Disentanglement for Concept-filtered Retrieval

One of the advantageous applications of SLiCS is the ability to conduct concept-filtered image retrieval. Accessing latent embeddings to measure the similarity between two images is easy and computationally cheap. When using a multilabel image as the query, by applying SLiCS to disentangle the embedding of the query, one can exploit a concept-filtered component to retrieve images based on a similarity scope focusing on a specific concept. Given a query embedding  $\mathbf{x}_*$ , concept-filtered retrieval based on the  $j$ th component uses the similarity score  $r_*^j = \cos(\tilde{\mathbf{v}}_j^*, \mathbf{x})$  for ranking a candidate image  $\mathbf{x}$ . The retrieval is based on ranking by sorting the pool of candidate images in descending order based on the similarity scores. As a baseline, unfiltered retrieval (UF-CLIP) uses the holistic similarity score  $r_* = \cos(\mathbf{x}_*, \mathbf{x})$ .

### 3.6 Word Captions of Subspaces

A set of words are selected to interpret the subspaces learned by SLiCS. We consider the single English word token from the captions of LAION-400m dataset, and follow Bhalla et al. [2024] to filter out any NSFW words and pick the most frequent 10,000 words. The text embeddings are normalized, mean-centered, and then re-normalized. Top 5 words that have the smallest non-negative linear reconstruction error using the concept dictionary  $\mathbf{B}_j$  are selected to describe the subspace  $\mathcal{V}_j$  since they are the closest to the subspace in the embedding space.

### 3.7 Image-to-prompt Visualization

Stable diffusion models often use a CLIP text embedding as the prompt to handle image generation. Ding et al. [2023] proposes a method to directly use an image embedding as the prompt. However, it requires that the image and text embeddings lie in the same contrastively learned latent space. Since the training of the stable diffusion model [Rombach et al., 2022] is conditioned on CLIP

ViT-L/14, it is necessary to align the image embedding spaces first. We formulate the space alignment problem as the well-known orthogonal Procrustes problem [Schönemann, 1966], which aims to find an orthogonal matrix that minimizes the mean-squared error as a regression problem between the embeddings. It has a closed-form solution in terms of the singular value decomposition of the product of the two embedding matrices. We choose Flickr30K dataset [Young et al., 2014], which contains 30,000 images with captions and is commonly used in cross-modal learning tasks, to align the spaces. The resulting orthogonal matrix is applied to  $\tilde{\mathbf{v}}_j^*$  as the prompt for the  $j$ th concept.

## 4 Experiments

### 4.1 Dataset and Preprocessing

We explore two instances of the CLIP model, corresponding to either ResNet-50 ( $\mathbf{x} \in \mathbb{R}^{1024}$ ) and ViT-B/32 ( $\mathbf{x} \in \mathbb{R}^{512}$ ) for the image embeddings. ViT-B/32 incorporates vision transformers. Except for the zero-shot concept classification, where the network’s original image embeddings are used, the image embeddings are first normalized to be unit norm, then centered with pre-computed mean from Bhalla et al. [2024] based on the gap between the distributions of image and text embeddings of CLIP [Liang et al., 2022], before being re-normalized to unit norm again.

In addition to the vision-language model, we also explore TiTok-L-32 [Yu et al., 2024], a vision transformer-based autoencoder that compresses input image into 32 pre-quantized tokens of dimension  $d$ ,  $\phi(X) \in \mathbb{R}^{32 \times d}$ . We vectorize the tokens to get the embedding  $\mathbf{x} \in \mathbb{R}^{384}$  when  $d = 12$ . Instead of normalizing across the whole embedding, we normalize each token separately to preserve the information each contains. Since there is no paired text encoder, no mean is removed from the embeddings. Another self-supervised distilled image feature extraction model with vision transformer as the backbone, DINOv2 ViT-B/14 [Jose et al., 2024], is explored. The embeddings, similar to that of CLIP, are vectors  $\mathbf{x} \in \mathbb{R}^{768}$ , which we also normalize without subtracting any mean.

MIRFlickr25K [Huiskes and Lew, 2008] and MS COCO [Lin et al., 2014] are used as the datasets. MIRFlickr25K contains  $N = 25,000$  images with  $S = 11$  general concepts—6 concepts have finer-grained labels. We use only the training set of MS COCO, which contains  $N = 118,000$  images, 80 finer-grained labels under  $S = 12$  general concepts. We delete images with all zero labels from both datasets. 2,000 images from MIRFlickr25K and 20,000 images from MS COCO are chosen as the training set, respectively. Both datasets have a disjoint validation set of 500 images and a query set of 1,000 images used as queries for the retrieval performance. The rest of each database constitutes the candidate images for retrieval.

### 4.2 Effect of Dictionary Size

The size of the dictionary in supervised and unsupervised SLiCS influences the ability to achieve meaningful disentanglement. Too few atoms limit the dictionary from capturing the diversity associated to a concept, while too many will lead to concept overlap, which limits the single concept “projection” from providing meaningful disentanglement.

From Fig. 2(b), it is clear that the disentanglement constructs a cluster-like representation of subspaces. Within each concept-specific subspace, we can use finer-grained concepts not known during training to see how organized or structured it is. That is, during dictionary learning no sub-level information is given, but is only used in assessment. The visualization in Fig. 3 shows how information is encoded in a subspace by the relative contribution of two atoms associated to the “animal” subspace.

A visualization of the image embeddings and disentangled components by t-SNE is shown in Fig. 4.

With an increasing  $d_0$ , the clusters that represent the finer-grained concepts first become separated and then merge together. At the extremes, too few atoms serving as prototypes prevent the subspace from capturing complex structure, but still enable it to disentangle different components, but too many atoms fail at both. When  $d_0 = 20$ , different clusters associated to the sub-label are not well separated from each other, leading to possible inaccurate retrieval. Therefore, an optimal dictionary size for retrieval lies between the two.

To emphasize that the group structure creates atoms that work together, coefficients are estimated without using the concept labels using greedy sparse coding (Orthogonal Matching Pursuit [Mallat and Zhang, 1993, Rubinstein et al., 2008] with non-negative constraint) across the validation set

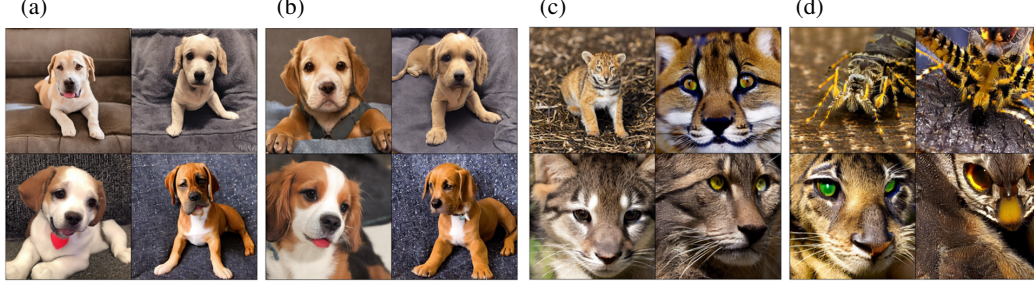


Figure 3: Generated images from image-to-prompt [Ding et al., 2023] applied to disentanglement in terms of two atoms  $\mathbf{b}_1, \mathbf{b}_2$  from the “animal” subspace. (a)  $0.25\mathbf{b}_1 + 0.75\mathbf{b}_2$ . (b)  $0.5\mathbf{b}_1 + 0.5\mathbf{b}_2$ . (c)  $0.75\mathbf{b}_1 + 0.25\mathbf{b}_2$ . (d)  $\mathbf{b}_1$ . As the coefficients change, the content of the generated images transition from dog, associated to  $\mathbf{b}_2$ , to feline and spider-like animals with more intense colors and striping, associated to  $\mathbf{b}_1$ .

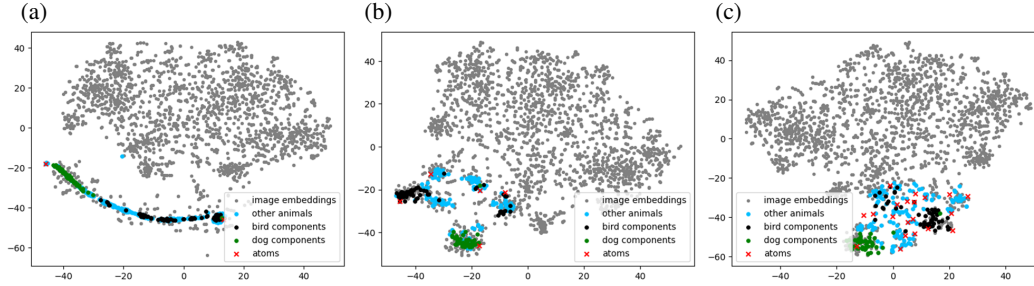


Figure 4: Visualization of disentangled subspaces by supervised SLiCS, with points corresponding to images with the “animal” concept colored using partial sub-label information. (a)  $d_0 = 2$  shows the subspace is a curve between two atoms. (c)  $d_0 = 5$  shows cluster structure within the subspace with the animal components that have “dog” or “bird” mostly within their own clusters. (d)  $d_0 = 20$  shows less clustering as more atoms allows a varied landscape of components, but “bird” and “dog” remain grouped.

examples. Then the co-occurrence between atoms is calculated from the frequency that one atom co-occurs with another based on both having non-zero coefficients. Fig. 5 shows that the group structure is evident from the co-occurrence matrix, whereas the atoms within a concept group are nearly orthogonal (as seen by the cosine similarity). During training, atoms associated to one concept are always allowed to co-occur compared to atoms from other concepts; thus, they tend to be nearly orthogonal to better capture the diversity within a concept.

### 4.3 Interpretation via Word Captions

Table 1: Subspace captions of MS COCO on CLIP ViT-B/32 embeddings. “Subspace” column shows the ground truth concept label. Words are ordered by the ascending reconstruction error.

Subspace	Supervised-SLiCS word caption	Unsupervised-SLiCS word caption
person	kid, kids, queen, granddaughter, daughter	granddaughter, kid, grandson, daughter, himself
vehicle	bike, bus, boats, boat, aircraft	transport, transportation, touring, truck, motorbike
outdoor	bench, benches, downtown, streets, hometown	downtown, snow, streets, snowfall, tourists
animal	dogs, pups, horses, cows, puppies	horse, cow, horses, bear, dogs
accessory	travelers, luggage, baggage, travel, travelling	packing, luggage, baggage, suitcase, travelling
sports	batting, flying, hikers, baseball, skiing	kids, surfers, children, childrens, baseball
kitchen	beverages, drinks, breakfast, alcohol, beverage	kitchen, kitchens, bathroom, cooking, workspace
food	veggies, vegetables, pizza, cake, sandwich	meal, desserts, breakfast, healthy, cake
furniture	room, bedroom, bedrooms, bed, toilet	furniture, lounge, beds, packing, workspace
electronic	office, workspace, television, tv, phone	phone, airplanes, midnight, plane, nights
appliance	kitchen, kitchens, bathroom, sinks, refrigerator	aircraft, toilet, plane, landed, locomotive
indoor	library, books, bookshelf, libraries, decor	hall, basement, museum, warehouse, stores

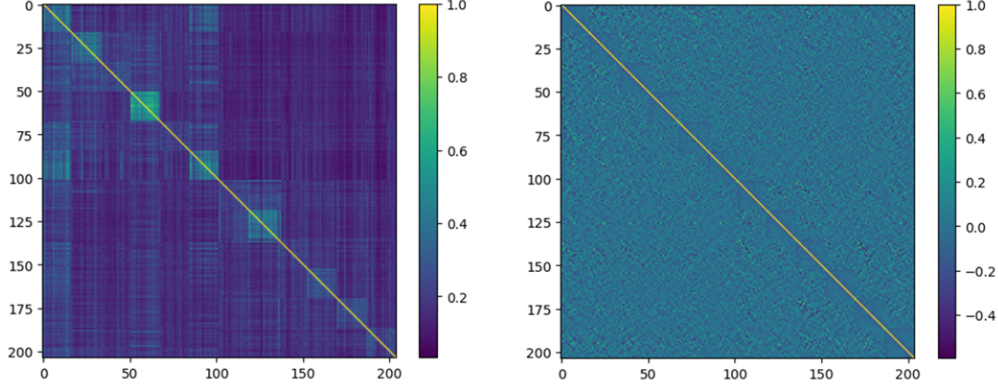


Figure 5: Relationship between the atoms across the concept dictionaries and their coefficients in supervised SLiCS. Dimensionality chosen by retrieval performance on validation set (see Section 4.4). (Left) the co-occurrence matrix of active atoms for images in the validation set. Each row is normalized separately so that the diagonal entries are 1. Within each group the co-occurrence rate is generally higher than between groups. (Right) The cosine similarity matrix of the atoms in the same dictionary. The within-group similarity ( $-0.056 \pm 0.062$ ) is slightly lower than cross-group similarity ( $0.000 \pm 0.134$ ).

The word captions of supervised and unsupervised SLiCS with ViT-B/32 embeddings are presented in Table 1. As shown in the tables, both supervised and unsupervised subspace disentanglement show semantic consistency. However, unsupervised word caption lists seem less disentangled. For example, “aircraft”, “plane”, and “airplanes” are assigned in “electronic” and “appliance”, possibly due to the inaccurate pseudo-labels due to photos within airplane cockpits or cabins containing electronics or appliances. As another example, “workspace” is shared by “kitchen” and “furniture”.

#### 4.4 Filtered and Unfiltered Retrieval

We carry out a concept-filtered retrieval to prove the efficacy of SLiCS. For a given concept  $j$  (general label) and a query where the concept is present, the task is to retrieve images where  $j$  is also present. A finer-grained concept-filtered retrieval score is also computed, where it is required to retrieve images that not only contain  $j$  but also contain the same finer-grained concept (sub-label) of the query. For example, if the query contains “dog”, but  $j$  is coarse grained, such that it denotes “animal”, then in normal concept-filtered retrieval, the relevant images are ones that also have “animal”, while in finer-grained retrieval, a returned image is only considered relevant when the image contains “dog”.

The retrieval is quantitatively measured by mean average precision of the top-20 retrieved images (mAP@ 20). It should be noted that for different  $j$ , the same query image may appear as query for different concepts. With the intuition explained in 3.3, we select the hyperparameter  $d_0$  in supervised SLiCS by comparing the finer-grained concept-filtered retrieval performance on a validation set. The optimal  $d_0$  and the performances of general label retrieval and sub-label retrieval on different embeddings are shown in Fig. 6.

For unsupervised SLiCS,  $\tilde{S}$  is estimated by calculating the average number of concepts per sample across the whole dataset. The average number of concepts  $\tilde{S}$  in MIRFlickr25K and MS COCO is 2.467 and 2.303. Hence, we pick  $\tilde{S} = 2$  for both datasets. We use the same  $d_0$  that was selected for supervised SLiCS for a fair comparison.

In both supervised and unsupervised SLiCS, (S-SLiCS and U-SLiCS), we apply standard dictionary training on MIRFlickr25K, while applying the mini-batch training on MS COCO with a batch size of 2,000. Both are trained for 10 iterations. As an internal baseline, we use the initialization step of supervised SLiCS to create a supervised SVD-based dictionary (S-SVD).

We compare our method against unfiltered retrieval with CLIP (UF-CLIP) and SpLiCE [Bhalla et al., 2024]. SpLiCE can either be used as an unfiltered retrieval method by reconstructing the image embedding based on the decomposed sparse coefficient, or as a filtered retrieval method by partially

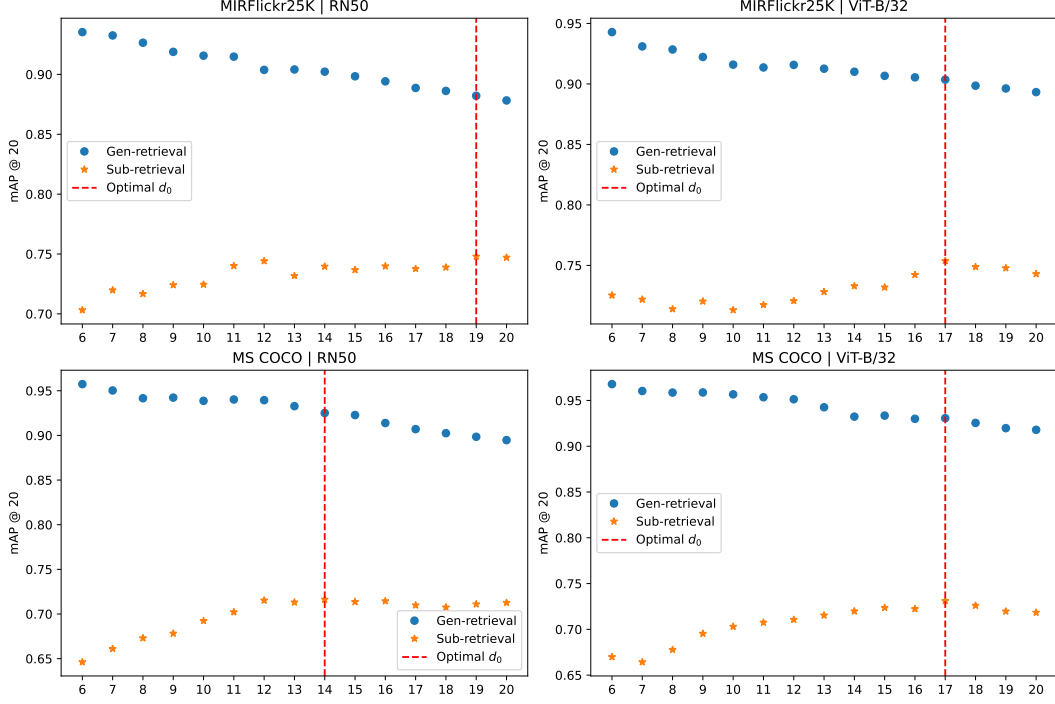


Figure 6: mAP @ 20 of general label retrieval and sub-label retrieval with various  $d_0$  on the validation set of different embeddings.  $d_0$  is searched from 5 to 20. The chosen  $d_0$  is denoted by the vertical line.

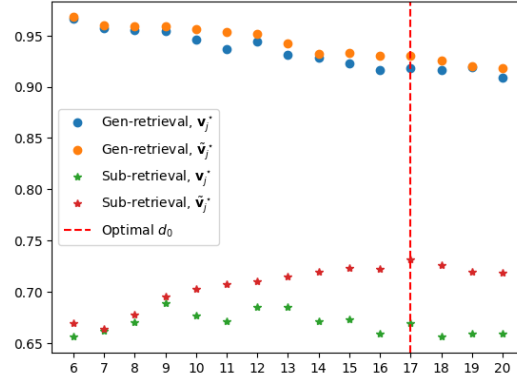


Figure 7: mAP @ 20 of general label retrieval and sub-label retrieval with various  $d_0$  on ViT-B/32 embeddings of MS COCO using  $v_j^*$  and  $v_j^{\sim}$ . The chosen  $d_0$  is denoted by the vertical line.

reconstructing the embedding to yield concept-specific components after the initial sparse coefficients decomposition, if a group structure of the word tokens is provided (F-SpLiCE). For F-SpLiCE, we group the tokens by assigning each to the closest centered concept word token  $w_i$  in terms of cosine similarity.

We present the quantitative results in Table 2 (CLIP embeddings). S-SLiCS models perform the best on all but one case. The proposed initialization S-SVD is best on that case and second best on the remaining cases. The direct comparison between S-SLiCS and S-SVD shows the iterations of the dictionary learning algorithm consistently improve general label retrieval (increased mAP@20 by 0.011, 0.015, 0.014, and 0.024 for the 4 cases) and usually improve sub-label retrieval (differences of 0.021, -0.001, 0.043, and 0.066). Compared to unfilted retrieval, S-SLiCS greatly improves general



Table 2: Quantitative results (mAP@20) for CLIP embeddings. **Gen.** denotes general label retrieval score; **Sub.** denotes sub-label retrieval score. **S-SVD**: subspaces learned from supervised SVD initialization. **S-SLiCS**: supervised SLiCS. **U-SLiCS**: unsupervised SLiCS. **UF-CLIP**: CLIP unfiltered retrieval baseline. **F-SpLiCE**: filtered retrieval using SpLiCE. **SpLiCE**: unfiltered retrieval using SpLiCE. The best performance across each row is marked in bold and second best is underlined.

Type		S-SVD	S-SLiCS	U-SLiCS	UF-CLIP	F-SpLiCE	SpLiCE
MIR/RN	Gen.	<u>0.864</u>	<b>0.875</b>	0.832	0.723	0.653	0.646
	Sub.	<u>0.735</u>	<b>0.756</b>	0.726	0.700	0.565	0.578
MIR/ViT	Gen.	<u>0.880</u>	<b>0.895</b>	0.862	0.728	0.702	0.669
	Sub.	<b>0.757</b>	<u>0.756</u>	0.729	0.700	0.607	0.612
COCO/RN	Gen.	<u>0.908</u>	<b>0.922 ± 0.001<sup>a</sup></b>	0.865 ± 0.037	0.782	0.628	0.707
	Sub.	<u>0.674</u>	<b>0.717 ± 0.003</b>	0.653 ± 0.005	0.663	0.496	0.584
COCO/ViT	Gen.	<u>0.905</u>	<b>0.929 ± 0.002</b>	0.871 ± 0.036	0.791	0.684	0.737
	Sub.	<u>0.676</u>	<b>0.742 ± 0.002</b>	0.672 ± 0.002	0.671	0.539	0.627

<sup>a</sup>SLiCS is deterministic if the order of the input is fixed. However, for MS COCO, we perform the mini-batch learning, which randomize the order of the batches at each iteration. The mean and standard deviation are calculated across five runs for MS COCO.

retrieval (0.152, 0.167, 0.14, 0.138) and moderately improves sub-label retrieval (0.056, 0.056, 0.054, 0.071). Sub-label retrieval is more difficult than general label retrieval, but SLiCS shows the potential to improve fine-grained image retrieval even when only general labels are given.

Except for COCO/RN sub-label, the unsupervised SLiCS (U-SLiCS) models perform third best. U-SLiCS performs well in general label retrieval (outperforming UF-CLIP by 0.109, 0.134, 0.083, and 0.08 across the 4 cases). For sub-label retrieval, U-SLiCS outperforms UF-CLIP on MIRFlickr25K by 0.026 and 0.029, but matches it on MS COCO. These results highlight the utility using pseudo-labels from zero-shot classification to enable unsupervised SLiCS for concept-filtered image retrieval.

Finally, we note that unfiltered CLIP always outperforms either of the SpLiCE baselines. SpLiCE’s unfiltered approximation does not achieve disentanglement, and the post-hoc grouping of atoms in F-SpLiCE based on similarity to the concept text embedding does not help.

#### 4.4.1 TiTok Embeddings

To show the wider applicability of SLiCS, we apply it to the latent “token” embeddings from TiTok ( $T_T = 32$  tokens, each  $d_T = 12$  dimensions, with a codebook  $\{\mathbf{c}_k\}_{k=1}^K = \mathcal{C}$  of size  $K = 4096$  for quantization). The embedding representation consists of the concatenation of the tokens  $d = T_T \cdot d_T = 32 \cdot 12 = 384$  after each is  $\ell_2$ -normalized but before each token is quantized. In Table 3, we present the results of supervised SLiCS and unfiltered TiTok embeddings. Quantitative results show that SLiCS provides much higher precision compared to unfiltered retrieval increases of mAP@20 with increases of 0.21 and 0.23 for general labels, and increases of 0.08 and 0.04 for sub-labels. The supervised SVD initialization actually outperforms the learned dictionary on 3 of the 4 cases. This indicates that for the TiTok embedding space, which was not trained with InfoNCE objective like CLIP, the non-negativity constraint which yields positive cones may not be necessary compared to linear subspaces. Nonetheless, these results highlight the importance of using disentanglement to provide meaningful retrieval.

We note that quantization can reduce the computation and storage when retrieving from a large pool of quantized embeddings of the candidate images. Let  $\mathbf{x} = [\mathbf{x}^t]_{t=1}^{T_T} \in \mathbb{R}^d$ ,  $\mathbf{x}^t \in \mathbb{R}^{d_T}$  denote the concatenation of normalized tokens for a candidate image. The quantization is

$$\tilde{\mathbf{x}} = \arg \min_{\mathbf{c} \in \mathcal{C} \times \dots \times \mathcal{C}} \|\mathbf{x} - \mathbf{c}\|_2, \quad \tilde{\mathbf{x}} = [\tilde{\mathbf{x}}^t]_{t=1}^{T_T}, \quad \tilde{\mathbf{x}}^t = \mathbf{c}_{k^t} = \arg \min_k \|\mathbf{x}^t - \mathbf{c}_k\|_2,$$

as in product quantization [Jegou et al., 2010]. The codebook vectors are also  $\ell_2$ -normalized such that  $\|\mathbf{c}\|_2 = 1$ ,  $\forall \mathbf{c} \in \mathcal{C}$ . The similarity score for the  $j$ th component  $\tilde{\mathbf{v}}_j^* = [\tilde{\mathbf{v}}_j^{*t}]_{t=1}^{T_T}$  using a quantized pool is then  $\tilde{r}_*^j = \cos(\tilde{\mathbf{v}}_j^*, \tilde{\mathbf{x}}) \propto \sum_{t=1}^{T_T} \tilde{\mathbf{v}}_j^{*t\top} \tilde{\mathbf{x}}^t = \sum_{t=1}^{T_T} \tilde{\mathbf{v}}_j^{*t\top} \mathbf{c}_{k^t} = \sum_{t=1}^{T_T} G_{t,k^t}^j$ , where  $\mathbf{G}^j = [\tilde{\mathbf{v}}_j^{*t\top} \mathbf{c}_k]_{t=1, k=1}^{T_T, K}$  is a look-up table that can be computed for a query’s component and codebook. The unfiltered by score for quantized pool is  $\tilde{r}_* = \cos(\mathbf{x}^*, \tilde{\mathbf{x}}) = \sum_{t=1}^{T_T} G_{t,k^t}$ , where  $\mathbf{G} = [\mathbf{x}^{*t\top} \mathbf{c}_k]_{t=1, k=1}^{T_T, K}$ . Computing the scores requires on the order of  $NT_T$  compared to  $NT_T d_T$

Table 3: Quantitative results (mAP@20) for TiTok embeddings. **Gen.** denotes general label retrieval score; **Sub.** denotes sub-label retrieval score. **S-SVD**: subspaces learned from supervised SVD initialization. **S-SLiCS**: supervised SLiCS applied to TiTok embeddings. **UF-TiTok**: TiTok unfiltered retrieval. For S-SLiCS and UF-TiTok, results are made from original (Not quant.) or quantized embeddings for the candidate pool images (Quant. pool). The mean and standard deviation are calculated across five runs for MS COCO. The best performance without quantization and the best within quantization in each row are each marked in bold and second best are underlined.

Type		S-SVD (TiTok)		S-SLiCS (TiTok)		UF-TiTok	
		No quant.	Quant. pool	No quant.	Quant. pool	No quant.	Quant. pool
MIR	Gen.	<u>0.724</u>	<u>0.715</u>	<b>0.738</b>	<b>0.724</b>	0.523	0.515
	Sub.	<b>0.516</b>	<b>0.519</b>	0.500	<u>0.484</u>	0.426	0.408
COCO	Gen.	<b>0.823</b>	<b>0.814</b>	<u>0.795</u> $\pm$ 0.004	<u>0.782</u> $\pm$ 0.003	0.564	0.553
	Sub.	<b>0.421</b>	<b>0.421</b>	<u>0.382</u> $\pm$ 0.005	<u>0.376</u> $\pm$ 0.002	0.341	0.322

without quantization; additionally, storing the candidate pool embeddings requires  $NT_T$  indices compared to  $NT_T d_T$  floating point numbers without quantization. The results in Table 3 show small drops in performance. Indicating that the retrieval is robust to the distortion brought by the quantization.

Similarly, the query could also be quantized. If the disentangled components of the query needs to stored or communicated, then the existing codebook is not appropriate as its entries are unit-norm, while  $\|\tilde{\mathbf{v}}_j^*\|_2 \leq 1$ . A new codebook, or concept-specific codebooks, should be learned to quantize  $\tilde{\mathbf{v}}_j^*$ ,  $j \in \mathcal{J}$ . Future work could investigate the most efficient mechanism. One option would be to exploit the existing codebook and further quantize the vector of scales  $\mathbf{g}_j = [g_{j,t}]_{t=1}^{T_T}$ .  $\tilde{\mathbf{v}}_j^* \approx [\tilde{\mathbf{c}}_{k^{j,t}}]_{t=1}^{T_T}$  where  $\tilde{\mathbf{c}}_{k^{j,t}} = g_{j,t} \mathbf{c}_{k^{j,t}}$  and  $(g_{j,t}, \mathbf{c}_{k^{j,t}}) = \arg \min_{g \geq 0, \mathbf{c} \in \mathcal{C}} \|\tilde{\mathbf{v}}_j^* - g\mathbf{c}\|_2$ . Each entry could be quantized separately. Ideally, the energy in components would isolated into a subset tokens such that the scales would be nearly binary such that component-tokens that are low-norm could be dropped and the component-tokens well-approximated with nearly unit-norm would be used.

#### 4.4.2 DINO Embeddings

We also apply SLiCS to the embeddings of the self-supervised DINOv2 ViT-B/14 model [Jose et al., 2024], which creates embeddings of images using a vision transformer backbone. The results of supervised SLiCS and unfiltered DINO embeddings are presented in Table 4.

Table 4: Quantitative results (mAP@20) for DINO embeddings. **Gen.** denotes general label retrieval score; **Sub.** denotes sub-label retrieval score. **S-SVD**: subspaces learned from supervised SVD initialization. **S-SLiCS**: supervised SLiCS applied to DINO embeddings. **UF-DINO**: DINO unfiltered retrieval. The mean and standard deviation are calculated across five runs for MS COCO. The best performance across each row is marked in bold and second best is underlined.

Type		S-SVD (DINO)	S-SLiCS (DINO)	UF-DINO
MIR	Gen.	<u>0.912</u>	<b>0.943</b>	0.726
	Sub.	<u>0.737</u>	<b>0.758</b>	0.700
COCO	Gen.	<u>0.909</u>	<b>0.984 <math>\pm</math> 0.001</b>	0.793
	Sub.	<u>0.728</u>	<b>0.785 <math>\pm</math> 0.004</b>	0.698

The improvements S-SLiCS over unfiltered retrieval show the efficacy of disentanglement, and the improvements on S-SVD initialization shows the efficacy of our dictionary learning algorithm. It should be noted that mAP @ 20 with the disentanglement of DINO embeddings is better than that with the disentanglement of CLIP embeddings. We note that DINO’s self-supervision tries to extract latent embeddings that are invariant to augmentations. The resulting embeddings may capture various aspects that differentiate the whole contents. In comparison, the CLIP model can be seen as weakly supervised, as it is trained to capture the semantic information in the image to match the paired caption. The way CLIP encodes the images is restricted by semantics with the guidance of captions, the quality of which restrict its abilities [Gurung et al., 2025], while DINO tries to extract anything that is unique about an image.

#### 4.5 Qualitative Concept-Filtered Retrieval Results

The qualitative results on MS COCO queries of ViT-B/32 embeddings are shown in Fig. 8. Although UF-CLIP and F-SpLiCE are able to retrieve similar images with query, they are not able to separate apart different concepts to enable a more specific retrieval as S-SLiCS. More specifically, S-SLiCS accurately retrieves a child with clothes of similar colors (first query) and a cat of similar color pattern (second query). U-SLiCS, on the other hand, retrieves a cat of disparate colors and a child less similar to the query, despite both correct finer-grained concepts.



Figure 8: Qualitative results for on CLIP ViT-B/32 embeddings. The concepts within each method are sorted in descending cosine similarity between the disentangled components and the query. S-SLiCS shows effective decomposition of the query into relevant concepts. Unfiltered retrieval methods can only retrieve images based on the whole scene, for example, in the first row, “cow” and “person” need to co-occur with similar relative position. In contrast, SLiCS applies concept-filtered retrieval obtaining images with a similar cow and a similar person separately.

The qualitative results on MS COCO queries of TiTok-L-32 embeddings are shown in Fig. 9. We also show the reconstruction of the queries using TiTok encoder to display the distortions brought by the compressive encoding. Unfiltered TiTok retrieval yields images similar to queries in terms of low-level spatial features but not in terms of semantic contents, which reveals the limitations of using cosine similarity as the metrics on other models than CLIP. Specifically, in the second query, the fact that supervised SLiCS fails to retrieve the correct animal may be due to the information is distorted during encoding, as the reconstruction image yields a dog rather than a cat.

The qualitative results shown in Fig. 10 further corroborates the disentanglement of the DINO embeddings. Concept-filtered retrieval accurately retrieves images with objects aligned with the concept in the query: the first query yields cow (“animal”) and kids (“person”), the second query yields black cat (“animal”) and suitcases (“accessory”), the third query yields man with a pair of sunglasses (“person”) and a cellphone being used (“electronic”).

#### 4.6 Visualizing Concept-Filtered Embeddings

The image-to-prompt realizations created using the concept-specific components of the query are shown in Fig. 11. While the TiTok decoder could be applied to the components of the query, as it was trained on unit-norm tokens, passing in tokens with less than unit-norm fails and quantization of the component-tokens with unit-norm codebook distorts the component and creates unnatural reconstructions. Like the compression of the components, this is left for future work.

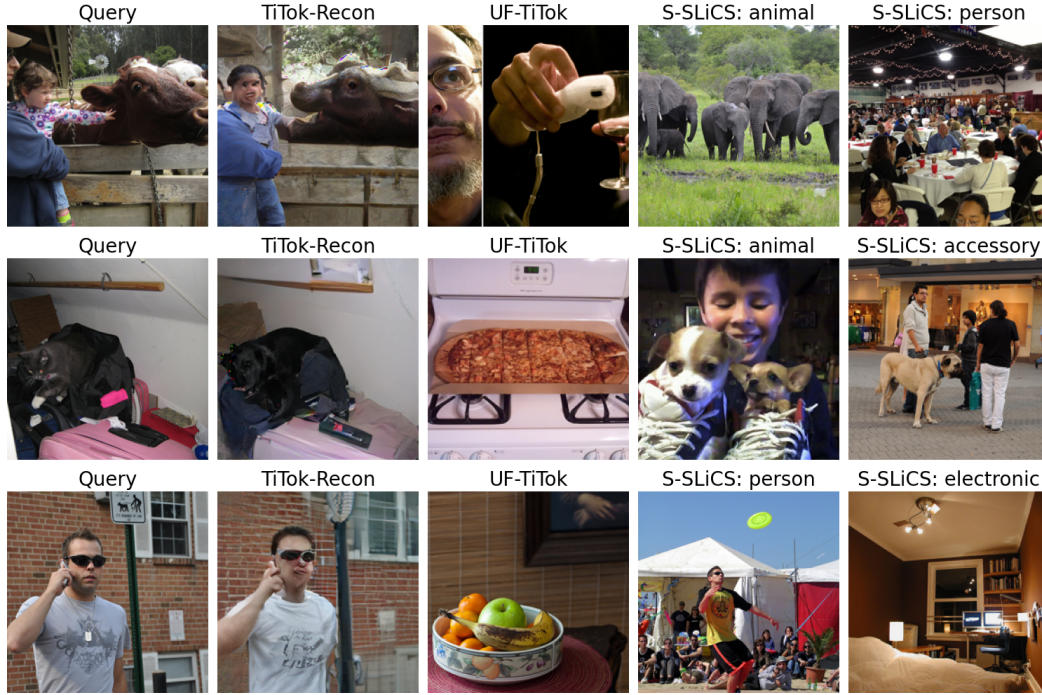


Figure 9: Qualitative results for on TiTok-L-32 embeddings. The concepts within each method are sorted in descending cosine similarity between the disentangled components and the query. **TiTok-Recon** column shows the TiTok reconstruction of the query images from the tokens, which bears distortions of varying degrees.

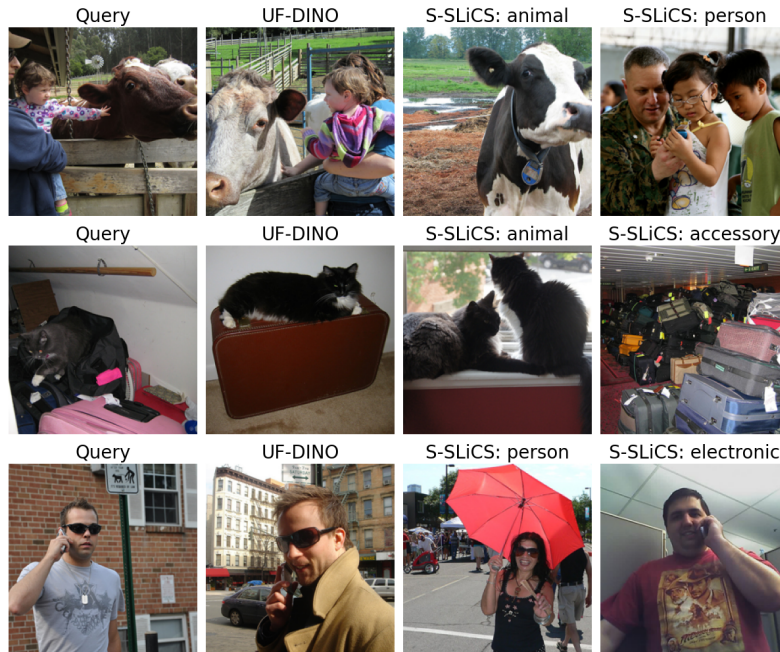


Figure 10: Qualitative results for on DINOv2 ViT-B/14 embeddings. The concepts within each method are sorted in descending cosine similarity between the disentangled components and the query.



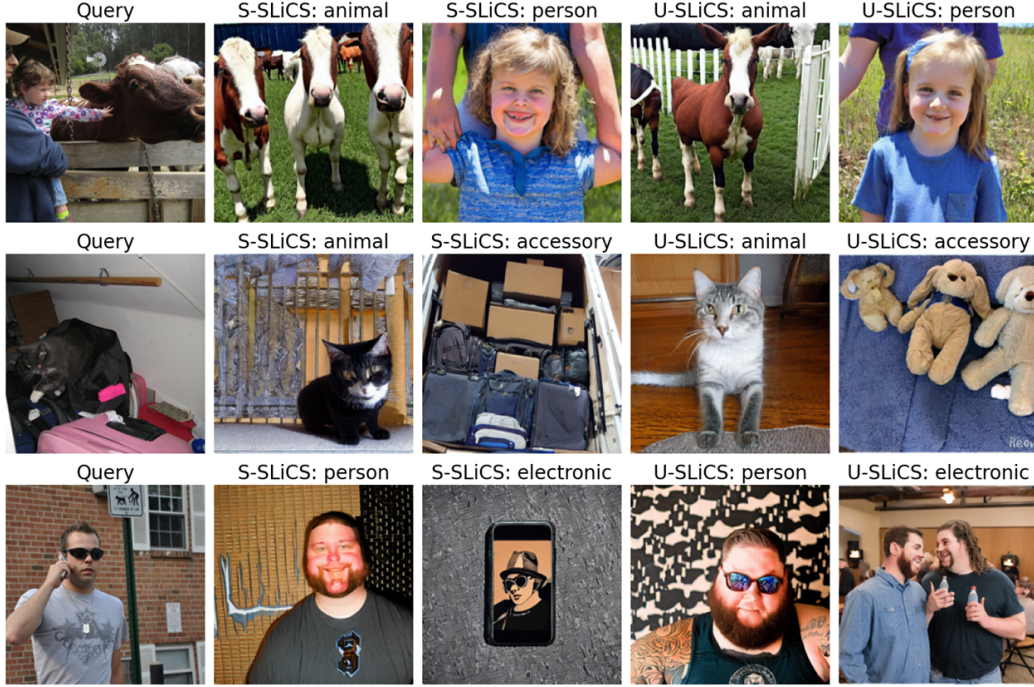


Figure 11: Image-to-prompt visualization for SLiCS model. The generated images in each row correspond to the components of each query in Fig. 8.

## 5 Conclusion

SLiCS enables the decomposition of CLIP image embeddings into meaningful concept subspaces with interpretable descriptions. The methods uses dictionary learning with supervision from labels or pseudo-labels obtained without supervision from zero-shot classification, with minimal guidance from the text embeddings of a known set of concepts. The immediate benefit of the decomposition is an effective concept-filtered image retrieval (0.895 mAP@20 on MIRFlickr25K and 0.929 on MS COCO) . The consistent word captions in both supervised and unsupervised cases offer insight into the structure of the CLIP embedding space and explore cross-modal interpretability.

SLiCS is also applicable to other vision embedding models. In particular, we examined the TiTok model trained as an highly compressive autoencoder with reconstruction loss and an adversarial critic as in VQGAN [Esser et al., 2021] to minimize the divergence between reconstructions and real images. While its baseline unfiltered retrieval was poor (0.523 mAP@20 on MIRFlickr25K and 0.564 on MS COCO) compared to CLIP (0.728 mAP@20 on MIRFlickr25K and 0.791 for MS COCO), using SLiCS the concept-filtered retrieval improved markedly (0.738 mAP@20 on MIRFlickr25K and 0.795 on MS COCO). Finally, we evaluated on DINOv2 [Jose et al., 2024] that uses self-supervised training to capture rich information from images. Remarkably, its unfiltered retrieval performance matched CLIP’s performance, and applying SLiCS to DINO embeddings yielding precise concept-filtered retrieval (0.943 mAP@20 on MIRFlickr25K and 0.984 on MS COCO). That shows that even though vision-language models are able to enable the text embeddings to describe the disentangled subspaces, an all-encompassing feature extraction model can have more advantages on image embeddings.

The feasibility of concept-level disentanglement indicates a promising and viable perspective to use a non-negative, group-sparse linear synthesis model to understand the latent embeddings of vision-language models and other deep neural networks.

## Acknowledgments and Disclosure of Funding

Research at the University of Delaware was sponsored by the Department of the Navy, Office of Naval Research under ONR award number N00014-24-1-2259. This material is based upon work supported by the National Science Foundation under Award No. 2108841. This research was supported in part through the use of Information Technologies (IT) resources at the University of Delaware, specifically the high-performance computing resources.

## References

- M. Aharon, M. Elad, and A. Bruckstein. K-SVD: An algorithm for designing overcomplete dictionaries for sparse representation. *IEEE Transactions on Signal Processing*, 54(11):4311–4322, 2006. doi: 10.1109/TSP.2006.881199.
- Alberto Baldrati, Marco Bertini, Tiberio Uricchio, and Alberto Del Bimbo. Effective conditioned and composed image retrieval combining CLIP-based features. In *2022 IEEE/CVF Conference on Computer Vision and Pattern Recognition (CVPR)*, pages 21434–21442, 2022. doi: 10.1109/CVPR52688.2022.02080.
- Usha Bhalla, Alex Oesterling, Suraj Srinivas, Flavio P. Calmon, and Himabindu Lakkaraju. Interpreting CLIP with sparse linear concept embeddings (SpLiCE). In A. Globerson, L. Mackey, D. Belgrave, A. Fan, U. Paquet, J. Tomczak, and C. Zhang, editors, *Advances in Neural Information Processing Systems*, volume 37, pages 84298–84328. Curran Associates, Inc., 2024. URL [https://proceedings.neurips.cc/paper\\_files/paper/2024/file/996bef37d8a638f37bdfcac2789e835d-Paper-Conference.pdf](https://proceedings.neurips.cc/paper_files/paper/2024/file/996bef37d8a638f37bdfcac2789e835d-Paper-Conference.pdf).
- Rasmus Bro and Sijmen De Jong. A fast non-negativity-constrained least squares algorithm. *Journal of Chemometrics*, 11(5):393–401, 1997. doi: [https://doi.org/10.1002/\(SICI\)1099-128X\(199709/10\)11:5<393::AID-CEM483>3.0.CO;2-L](https://doi.org/10.1002/(SICI)1099-128X(199709/10)11:5<393::AID-CEM483>3.0.CO;2-L). URL <https://analyticalsciencejournals.onlinelibrary.wiley.com/doi/abs/10.1002/%28SICI%291099-128X%28199709/10%2911%3A5%3C393%3A%3AAID-CEM483%3E3.0.CO%3B2-L>.
- J-F Cardoso. Multidimensional independent component analysis. In *Proceedings of the 1998 IEEE International Conference on Acoustics, Speech and Signal Processing, ICASSP'98 (Cat. No. 98CH36181)*, volume 4, pages 1941–1944. IEEE, 1998.
- Mathilde Caron, Ishan Misra, Julien Mairal, Priya Goyal, Piotr Bojanowski, and Armand Joulin. Unsupervised learning of visual features by contrasting cluster assignments. *Advances in neural information processing systems*, 33:9912–9924, 2020.
- Chandramani Chaudhary, Poonam Goyal, Navneet Goyal, and Yi-Ping Phoebe Chen. Image retrieval for complex queries using knowledge embedding. *ACM Trans. Multimedia Comput. Commun. Appl.*, 16(1), mar 2020. ISSN 1551-6857. doi: 10.1145/3375786. URL <https://doi.org/10.1145/3375786>.
- Ting Chen, Simon Kornblith, Mohammad Norouzi, and Geoffrey Hinton. A simple framework for contrastive learning of visual representations. In *International Conference on Machine Learning*, pages 1597–1607. PMLR, 2020a.
- Xinlei Chen, Haoqi Fan, Ross Girshick, and Kaiming He. Improved baselines with momentum contrastive learning. *arXiv preprint arXiv:2003.04297*, 2020b.
- Xinlei Chen, Saining Xie, and Kaiming He. An empirical study of training self-supervised vision transformers. In *Proceedings of the IEEE/CVF international conference on computer vision*, pages 9640–9649, 2021.
- Guillaume Couairon, Matthijs Douze, Matthieu Cord, and Holger Schwenk. Embedding arithmetic of multimodal queries for image retrieval. In *2022 IEEE/CVF Conference on Computer Vision and Pattern Recognition Workshops (CVPRW)*, pages 4946–4954, 2022. doi: 10.1109/CVPRW56347.2022.00542.
- Chris HQ Ding, Tao Li, and Michael I Jordan. Convex and semi-nonnegative matrix factorizations. *IEEE Transactions on Pattern Analysis and Machine Intelligence*, 32(1):45–55, 2008.
- Yuxuan Ding, Chunna Tian, Haoxuan Ding, and Lingqiao Liu. The CLIP model is secretly an image-to-prompt converter. In *Thirty-seventh Conference on Neural Information Processing Systems*, 2023. URL <https://openreview.net/forum?id=1Ha7gFbmVS>.
- Patrick Esser, Robin Rombach, and Bjorn Ommer. Taming transformers for high-resolution image synthesis. In *Proceedings of the IEEE/CVF Conference on Computer Vision and Pattern Recognition*, pages 12873–12883, 2021.

- Yossi Gandelsman, Alexei A. Efros, and Jacob Steinhardt. Interpreting CLIP’s image representation via text-based decomposition. In *The Twelfth International Conference on Learning Representations*, 2024. URL <https://openreview.net/forum?id=5Ca9sSzuDp>.
- Nicolas Gillis and Abhishek Kumar. Exact and heuristic algorithms for semi-nonnegative matrix factorization. *SIAM Journal on Matrix Analysis and Applications*, 36(4):1404–1424, 2015.
- Bijay Gurung, David T Hoffmann, and Thomas Brox. Clip won’t learn object-attribute binding from natural data and here is why. *arXiv preprint arXiv:2507.07985*, 2025.
- Michael Gutmann and Aapo Hyvärinen. Noise-contrastive estimation: A new estimation principle for unnormalized statistical models. In *Proceedings of the Thirteenth International Conference on Artificial Intelligence and Statistics*, pages 297–304. JMLR Workshop and Conference Proceedings, 2010.
- Arthur E Hoerl and Robert W Kennard. Ridge regression: Biased estimation for nonorthogonal problems. *Technometrics*, 12(1):55–67, 1970.
- Robert Huben, Hoagy Cunningham, Logan Riggs Smith, Aidan Ewart, and Lee Sharkey. Sparse autoencoders find highly interpretable features in language models. In *The Twelfth International Conference on Learning Representations*, 2024. URL <https://openreview.net/forum?id=F76bwRSLek>.
- Mark J. Huiskes and Michael S. Lew. The MIR Flickr retrieval evaluation. In *MIR ’08: Proceedings of the 2008 ACM International Conference on Multimedia Information Retrieval*, New York, NY, USA, 2008. ACM.
- Aapo Hyvärinen and Patrik Hoyer. Emergence of phase-and shift-invariant features by decomposition of natural images into independent feature subspaces. *Neural Computation*, 12(7):1705–1720, 2000.
- Herve Jegou, Matthijs Douze, and Cordelia Schmid. Product quantization for nearest neighbor search. *IEEE Transactions on Pattern Analysis and Machine Intelligence*, 33(1):117–128, 2010.
- Cijo Jose, Théo Moutakanni, Dahyun Kang, Federico Baldassarre, Timothée Darcet, Hu Xu, Shang-Wen Li, Marc Szafraniec, Michael Ramamonjisoa, Maxime Oquab, Oriane Siméoni, Huy V. Vo, Patrick Labatut, and Piotr Bojanowski. DINOv2 meets text: A unified framework for image- and pixel-level vision-language alignment. *2025 IEEE/CVF Conference on Computer Vision and Pattern Recognition (CVPR)*, pages 24905–24916, 2024. URL <https://api.semanticscholar.org/CorpusID:274981573>.
- Konstantin Kobs, Michael Steininger, and Andreas Hotho. InDiReCT: Language-guided zero-shot deep metric learning for images. In *2023 IEEE/CVF Winter Conference on Applications of Computer Vision (WACV)*, pages 1063–1072, 2023. doi: 10.1109/WACV56688.2023.00112.
- Victor Weixin Liang, Yuhui Zhang, Yongchan Kwon, Serena Yeung, and James Y Zou. Mind the gap: Understanding the modality gap in multi-modal contrastive representation learning. In S. Koyejo, S. Mohamed, A. Agarwal, D. Belgrave, K. Cho, and A. Oh, editors, *Advances in Neural Information Processing Systems*, volume 35, pages 17612–17625. Curran Associates, Inc., 2022. URL [https://proceedings.neurips.cc/paper\\_files/paper/2022/file/702f4db7543a7432431df588d57bc7c9-Paper-Conference.pdf](https://proceedings.neurips.cc/paper_files/paper/2022/file/702f4db7543a7432431df588d57bc7c9-Paper-Conference.pdf).
- Tsung-Yi Lin, Michael Maire, Serge Belongie, James Hays, Pietro Perona, Deva Ramanan, Piotr Dollár, and C. Lawrence Zitnick. Microsoft COCO: Common objects in context. In David Fleet, Tomas Pajdla, Bernt Schiele, and Tinne Tuytelaars, editors, *Computer Vision – ECCV 2014*, pages 740–755, Cham, 2014. Springer International Publishing. ISBN 978-3-319-10602-1.
- Zheyuan Liu, Cristian Rodriguez-Opazo, Damien Teney, and Stephen Gould. Image retrieval on real-life images with pre-trained vision-and-language models. In *2021 IEEE/CVF International Conference on Computer Vision (ICCV)*, pages 2105–2114, 2021. doi: 10.1109/ICCV48922.2021.00213.
- S.G. Mallat and Zhifeng Zhang. Matching pursuits with time-frequency dictionaries. *IEEE Transactions on Signal Processing*, 41(12):3397–3415, 1993. doi: 10.1109/78.258082.
- Maxime Oquab, Timothée Darcet, Théo Moutakanni, Huy Vo, Marc Szafraniec, Vasil Khalidov, Pierre Fernandez, Daniel Haziza, Francisco Massa, Alaaeldin El-Nouby, et al. DINOv2: Learning robust visual features without supervision. *arXiv preprint arXiv:2304.07193*, 2023.
- Yagyensh Chandra Pati, Ramin Rezaiifar, and Perinkulam Sambamurthy Krishnaprasad. Orthogonal matching pursuit: Recursive function approximation with applications to wavelet decomposition. In *Proceedings of 27th Asilomar Conference on Signals, Systems and Computers*, pages 40–44. IEEE, 1993.
- Ben Poole, Sherjil Ozair, Aaron Van Den Oord, Alex Alemi, and George Tucker. On variational bounds of mutual information. In *International Conference on Machine Learning*, pages 5171–5180. PMLR, 2019.

- Alec Radford, Jong Wook Kim, Chris Hallacy, Aditya Ramesh, Gabriel Goh, Sandhini Agarwal, Girish Sastry, Amanda Askell, Pamela Mishkin, Jack Clark, Gretchen Krueger, and Ilya Sutskever. Learning transferable visual models from natural language supervision. In Marina Meila and Tong Zhang, editors, *Proceedings of the 38th International Conference on Machine Learning*, volume 139 of *Proceedings of Machine Learning Research*, pages 8748–8763. PMLR, 18–24 Jul 2021. URL <https://proceedings.mlr.press/v139/radford21a.html>.
- Robin Rombach, Andreas Blattmann, Dominik Lorenz, Patrick Esser, and Björn Ommer. High-resolution image synthesis with latent diffusion models. In *Proceedings of the IEEE/CVF Conference on Computer Vision and Pattern Recognition (CVPR)*, pages 10684–10695, June 2022.
- Ron Rubinstein, Michael Zibulevsky, and Michael Elad. Efficient implementation of the K-SVD algorithm using batch orthogonal matching pursuit. Technical Report CS-2008-08, Technion - Computer Science Department, 2008. URL <https://csaws.cs.technion.ac.il/~ronrubin/Publications/KSVD-OMP-v2.pdf>.
- Peter H Schönemann. A generalized solution of the orthogonal procrustes problem. *Psychometrika*, 31(1):1–10, 1966.
- Martin Slawski and Matthias Hein. Non-negative least squares for high-dimensional linear models: Consistency and sparse recovery without regularization. *Electronic Journal of Statistics*, 7:3004–3056, 2013.
- P. Stoica and Y. Selen. Cyclic minimizers, majorization techniques, and the expectation-maximization algorithm: a refresher. *IEEE Signal Processing Magazine*, 21(1):112–114, 2004. doi: 10.1109/MSP.2004.1267055.
- Grzegorz Swirszcz, Naoki Abe, and Aurelie C Lozano. Grouped orthogonal matching pursuit for variable selection and prediction. *Advances in Neural Information Processing Systems*, 22, 2009.
- Aaron Van Den Oord, Oriol Vinyals, and koray kavukcuoglu. Neural discrete representation learning. *Advances in Neural Information Processing Systems*, 30, 2017.
- Laurens Van der Maaten and Geoffrey Hinton. Visualizing data using t-SNE. *Journal of Machine Learning Research*, 9(11), 2008.
- Ekaterina Vylomova, Laura Rimell, Trevor Cohn, and Timothy Baldwin. Take and took, gaggle and goose, book and read: Evaluating the utility of vector differences for lexical relation learning. *arXiv preprint arXiv:1509.01692*, 2015.
- Peter Young, Alice Lai, Micah Hodosh, and Julia Hockenmaier. From image descriptions to visual denotations: New similarity metrics for semantic inference over event descriptions. *Transactions of the Association for Computational Linguistics*, 2:67–78, 2014. doi: 10.1162/tac1\_a\_00166. URL <https://aclanthology.org/Q14-1006>.
- Qihang Yu, Mark Weber, Xueqing Deng, Xiaohui Shen, Daniel Cremers, and Liang-Chieh Chen. An image is worth 32 tokens for reconstruction and generation. *Advances in Neural Information Processing Systems*, 37: 128940–128966, 2024.
- Mert Yuksekgonul, Maggie Wang, and James Zou. Post-hoc concept bottleneck models. In *The Eleventh International Conference on Learning Representations*, 2023. URL <https://openreview.net/forum?id=nA5AZ8CEyow>.

## A Alternative update of atoms

In K-SVD, using SVD to simultaneously update coefficients and atoms during the atom update step is optimal to reduce the norm of the error in the residual. However, with an additional non-negative constraint, it is not optimal, as the problem is a rank-1 semi-NMF problem [Gillis and Kumar, 2015]. Rather than our heuristic, which uses the thresholded coefficients after identifying the optimal sign, an alternative is to perform block-coordinate descent by updating atom and coefficients separately. Given the previous coefficients, each entry of the atom can be optimized in parallel by ordinary least squares. Then, given updated atom, the non-negative linear regression can be used to obtain the updated coefficients, again in parallel:

$$\hat{\mathbf{b}}_m = \arg \min_{\gamma} \|\mathbf{E} - \gamma \beta_0\|_F^2, \quad \check{\beta} = (\check{\beta})_+, \quad \check{\beta} = \arg \min_{\beta} \|\mathbf{E} - \hat{\mathbf{b}}_m \beta\|_F^2, \quad (14)$$



where  $\beta_0 = [A_{ml}]_{l \in \mathcal{L}_m}$  from the previous coefficient update. Both of these problems have closed-form solutions,  $\acute{\mathbf{b}}_m = \mathbf{E}\beta_0^\top (\beta_0\beta_0^\top)^{-1} = \frac{\mathbf{E}\beta_0^\top}{\|\beta_0\|^2}$  and  $\check{\beta} = (\acute{\mathbf{b}}_m^\top \acute{\mathbf{b}}_m)^{-1} \acute{\mathbf{b}}_m^\top \mathbf{E} = \frac{\acute{\mathbf{b}}_m^\top \mathbf{E}}{\|\acute{\mathbf{b}}_m\|^2}$ , respectively.

With the inclusion of a normalizing step to enforce  $\acute{\mathbf{b}}_m$  to have unit norm, the solutions are scaled yielding

$$\acute{\mathbf{b}}_m = \frac{\mathbf{E}\beta_0^\top}{\|\mathbf{E}\beta_0^\top\|}, \quad \check{\beta} = (\acute{\mathbf{b}}_m^\top \acute{\mathbf{b}}_m)^{-1} \acute{\mathbf{b}}_m^\top \mathbf{E} = \frac{\beta_0 \mathbf{E}^\top \mathbf{E}}{\|\beta_0 \mathbf{E}^\top\|}. \quad (15)$$

Following Eq. 11, the residual error after the update is

$$\|\mathbf{E} - \acute{\mathbf{b}}_m(\check{\beta})_+\|_F^2 = \|\mathbf{E}\|_F^2 - \|(\check{\beta})_+\|_2^2. \quad (16)$$

The residual error can be lower bounded by upper bounding the second term as

$$\|(\check{\beta})_+\|_2^2 \leq \|\check{\beta}\|_2^2 = \frac{\|\beta_0 \mathbf{E}^\top \mathbf{E}\|_2^2}{\|\beta_0 \mathbf{E}^\top\|_2^2} \leq \left\| \frac{\beta_0 \mathbf{E}^\top}{\beta_0 \mathbf{E}^\top} \right\|_2^2 \cdot \|\mathbf{E}\|_{\text{op}}^2 = \sigma_1^2 = \|\check{\beta}\|_2^2. \quad (17)$$

Although it is hard to compare between  $\|(\check{\beta})_+\|$  and  $\|(p^* \check{\beta})_+\|$ , we know from (17) that the total norm of  $\check{\beta}$  is smaller than  $\check{\beta}$ , making it less likely to reduce more residual error. Furthermore, it also shows that at the beginning phase of the iteration, where  $\acute{\mathbf{b}}_m^\top$  is far apart from the space described by  $\mathbf{E}$ , the last inequality will be stronger. In fact, it is easy to show that when the true optimum is close, i.e., when  $\mathbf{E}$  can be well-approximated by a rank-1 matrix, these two methods are equal. Assuming  $\mathbf{E} = \sigma_1 \mathbf{u}_1^L \mathbf{u}_1^{R\top}$ , since  $\acute{\mathbf{b}}_m^\top$  needs to lie in the space of  $\mathbf{E}$ , which only has one left singular vector, leading to  $\acute{\mathbf{b}}_m^\top = \mathbf{u}_1^{L\top}$ , then

$$\check{\beta} = \sigma_1 \mathbf{u}_1^{L\top} \mathbf{u}_1^L \mathbf{u}_1^{R\top} = \sigma_1 \mathbf{u}_1^{R\top} = \check{\beta}. \quad (18)$$

Considering that new coefficients can be written in terms of previous coefficients, given the initial update of non-negative set of coefficients,  $\hat{\beta}_1 = (\check{\beta})_+$ , a heuristic approach is to iteratively update,

$$\hat{\beta}_{t+1} = \left( \frac{\hat{\beta}_t \mathbf{E}^\top \mathbf{E}}{\|\hat{\beta}_t \mathbf{E}^\top\|} \right)_+, \quad (19)$$

for  $t \in \{1, \dots, T\}$  as a modified power method.